Fusion Engineering and Design 202 (2024) 114325

Contents lists available at ScienceDirect

Fusion Engineering and Design

journal homepage: www.elsevier.com/locate/fusengdes

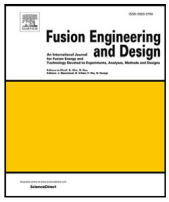

Numerical and experimental analysis of magneto-convective flows around pipes

C. Mistrangelo *, L. Bühler, C. Courtessole, C. Koehly

Karlsruhe Institute of Technology (KIT), P.O. Box 3640, 76021 Karlsruhe, Germany

ARTICLE INFO

Keywords:
Liquid metal breeder blankets
Magnetohydrodynamics (MHD)
Numerical simulations
Liquid metal experiments
Thermoelectric effects

ABSTRACT

Liquid metal flows exposed to intense magnetic fields play a fundamental role in the development of blankets for nuclear fusion reactors, where they serve to produce the plasma-fuel component tritium and transport the generated heat. When the liquid metal circulates in the blanket, it interacts with the plasma-confining magnetic field leading to the induction of electric currents. Electromagnetic forces and thermal buoyancy affect significantly velocity and pressure distributions. The resulting magneto-convective flow has peculiar features that have to be taken into account in order to evaluate heat transfer properties in the liquid metal. In the breeding zone of the water-cooled lead lithium blanket concept, the volumetric heat released in the liquid metal is removed by water-cooled circular pipes that represent obstacles for the liquid metal flow. In order to improve the understanding of the underlying physical phenomena and obtain a database for code validation, model experiments have been performed to investigate magneto-convective flow and heat transfer at two differentially heated parallel horizontal tubes immersed in a box filled with liquid metal. Among other properties, electric potential has been recorded on the surface of the test-section and compared with 3D numerical simulations. Computational results provide the basis for interpretation of the measured data, since they allow differentiating between flow-induced electric potential and thermoelectric effects.

1. Introduction

The buoyancy-driven flow of an electrically conducting fluid, such as a liquid metal, exposed to a magnetic field, represents a problem of fundamental importance in the development of blankets, which surround the hot deuterium–tritium plasma in nuclear fusion reactors [1,2]. Different liquid metal blanket concepts are currently under investigation and the water-cooled lead-lithium (WCLL) blanket has been selected as driver design for future use in a DEMOnstration fusion power plant [3]. In the WCLL blanket, the liquid metal alloy lead lithium (PbLi) is used as breeding material to produce the fuel component tritium and as heat transfer medium. PbLi has to be circulated in the breeding zones, to route it towards external systems for purification and tritium extraction. The motion of this electrically conducting fluid in the intense magnetic field, which confines the fusion plasma in a toroidal shape away from solid walls, induces electric currents and electromagnetic Lorentz forces that significantly affect flow features, such as velocity distribution, heat transfer properties, and pressure losses. These magnetohydrodynamic (MHD) phenomena, impact the feasibility and performance of a blanket design.

In the breeding zones of the WCLL blanket, the volumetric heat due to neutron irradiation is removed by a number of cooling pipes immersed in the liquid metal [4]. Therefore, since PbLi does not serve as coolant, the velocity of the forced flow can be minimized, so that the MHD-related pressure drop remains relatively small. However, even if additional MHD pressure losses do not represent a critical issue, the cooling pipes obstruct the liquid metal flow and lead to the occurrence of typical internal layers parallel to the magnetic field and tangent to the tubes [5]. This results in peculiar flow patterns that affect heat and mass transfer. Hence, the investigation of magneto-convective flows in the presence of submerged obstacles is essential to clarify aspects related to the cooling system efficiency in the WCLL blanket.

A large number of studies is available in literature, which focuses on classical configurations such as Rayleigh–Bénard convection [6] and differentially heated cavities with a horizontal temperature gradient [7]. Magneto convection in pipes and ducts has been studied by many authors, as described in an extensive review by Zikanov et al. (2021) [8]. On the other hand, the analysis of convective flows in geometries with internal obstacles did not receive much attention [5,9].

In the present paper, we discuss numerical results of magneto-convective flow in a model geometry that features two parallel pipes kept at constant differential temperatures, immersed in an adiabatic rectangular box filled with liquid metal, and we compare results with

* Corresponding author.
E-mail address: chiara.mistrangelo@kit.edu (C. Mistrangelo).

https://doi.org/10.1016/j.fusengdes.2024.114325
Received 3 October 2023; Received in revised form 12 January 2024; Accepted 6 March 2024
Available online 13 March 2024

experimental data. This configuration derives from a test-section used for experiments with the model fluid GaInSn performed in the MEKKA laboratory of the Karlsruhe Institute of Technology [10,11]. During the experimental campaign, electric potential has been recorded at more than 400 positions on the fluid-wall interface of the box. In case of isothermal experiments, the electric potential can be interpreted as a streamfunction for the flow and recorded electric potential differences can be regarded as approximate velocity components and used to gain insight into the flow distribution in the experimental test-section. The potential gradient approximates quite well the velocity components if the current density is small. This approach has been successfully applied to the analysis of different MHD flows [12,13]. Instead, in magneto-convective flows, the measurement of flow-induced electric potential is disturbed by the thermoelectric voltage that develops between two measuring points when there is a temperature difference between them [14,15]. Since the thermoelectric potential is expected to be of the same order of magnitude as the flow induced potential, numerical results are employed to give a suitable physical interpretation of the recorded data by taking into account the thermoelectric effects on the potential measurements in the experiments.

2. Problem definition

2.1. Numerical and experimental set-up

We consider the magneto-convective flow of a liquid metal in a rectangular box exposed to an externally applied uniform magnetic field $\mathbf{B} = -B\hat{\mathbf{y}}$ aligned with gravity $\mathbf{g} = -g\hat{\mathbf{y}}$. In the adiabatic and electrically insulating cavity, two horizontal differentially heated cylinders are inserted with their axes parallel to the coordinate x, as shown in Fig. 1a. The typical length $L = 0.05$ m of the problem is chosen as half of the distance between the walls perpendicular to the magnetic field, which are called Hartmann walls. This quantity is used to scale all lengths in the problem. In non dimensional notation the size of the computational domain in the three directions is defined by $-2 \le x = X/L \le 2, -1 \le y = Y/L \le 1$ and $-2 \le z = Z/L \le 2$. Walls parallel to the magnetic field are named side walls at $z = \pm 2$ and end-walls at $x = \pm 2$. The centers of the two cylinders are positioned at $z = \pm 1$ on the middle plane $y = 0$. The two pipes are kept at constant differential temperatures $T_{1,2} = T_0 \mp \Delta T$, given a mean temperature T_0 and a characteristic temperature difference ΔT. In the experiments, the mean temperature T_0 has been kept constant and as close as possible to the ambient temperature (30 °C), while adjusting $T_{1,2}$ to reach the chosen Grashof number Gr (see (5)). Simulations have been performed by following the same procedure. The temperature gradient in the fluid leads to the occurrence of buoyancy forces that drive convective motions in the liquid metal, while velocity-induced currents generate braking Lorentz forces.

In order to record electric potential during the experiments, thin copper electrodes are positioned on the top Hartmann wall (H) at $y = 1$ and on the end-wall (E) at $x = 2$. Fig. 1b shows a photograph of the test-section with electric potential sensors wired to the measuring system. Electric potential measurements are performed with respect to a reference point $\mathbf{x}_r$ located at $z = 0$ close to the center of the Hartmann wall (see Fig. 1b).

2.2. Mathematical formulation

The viscous incompressible flow of an electrically conducting fluid in a magnetic field and in presence of thermal gradients is driven by buoyancy and electromagnetic forces. It is mathematically described by equations for continuity of the velocity field, $\nabla \cdot \mathbf{v} = 0$, satisfying mass conservation, and by balance of momentum

$$\rho_0 \left(\frac{\partial}{\partial t} + \mathbf{v} \cdot \nabla \right) \mathbf{v} = -\nabla p + \rho_0 \nu \nabla^2 \mathbf{v} - \rho_0 \beta (T - T_0) \mathbf{g} + \mathbf{j} \times \mathbf{B}, \quad (1)$$

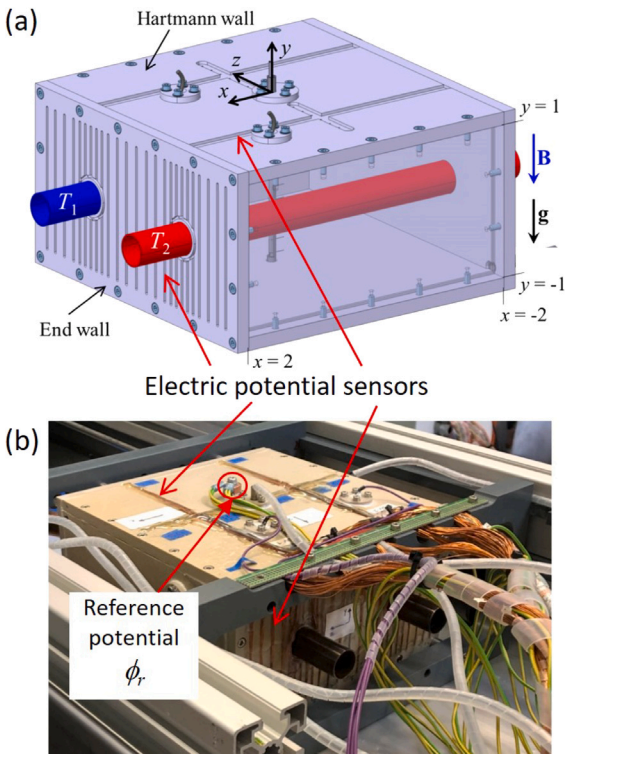

Fig. 1. Design of the test-section used for experiments, nondimensional sizes and coordinate system (a). Photograph of the manufactured and instrumented box (b).

where the distribution of the temperature T is described by the heat equation

$$\rho_0 c_p \left(\frac{\partial T}{\partial t} + (\mathbf{v} \cdot \nabla) T \right) - k \nabla^2 T = 0. \quad (2)$$

The variables $\mathbf{v}$, $\mathbf{j}$, $\mathbf{B}$, p and T indicate velocity, current density, applied magnetic field, pressure and temperature. Density changes in the liquid metal due to temperature variations are described in the buoyancy term in (1) by the Boussinesq approximation $\rho(T) = \rho_0 \left[1 - \beta (T - T_0)\right]$. The thermophysical properties of the fluid, i.e. reference density ρ_0, volumetric thermal expansion coefficient β, kinematic viscosity ν, specific heat c_p, thermal conductivity k and electric conductivity σ, are assumed to be constant and taken at the mean temperature $T_0 = (T_1 + T_2)/2$ [16].

Electric currents responsible for the electromagnetic Lorentz force result from Ohm's law

$$\mathbf{j}/\sigma = -\nabla \phi + \mathbf{v} \times \mathbf{B} - S \nabla T. \quad (3)$$

They are driven by the gradient of the electric potential ϕ, by the flow-induced electric field and by the thermoelectric electromotive force. The coefficient S multiplying the temperature gradient is known as the "absolute thermoelectric power of the conducting medium" [14] and since S is a function of T only, the third term on the right-hand side of Eq. (3) "is irrotational and incapable of driving currents wholly within such a medium" [17]. This allows replacing it with the gradient of a scalar function $W(T) = \int S dT$.

The Poisson equation

$$\nabla^2 \Phi = \nabla \cdot (\mathbf{v} \times \mathbf{B}) \quad (4)$$

ensures conservation of charge $\nabla \cdot \mathbf{j} = 0$ and if we regard $\Phi = \phi + W$ as a pseudo potential, the equations shown above do not differ from those of isothermal MHD flows. Thermoelectric effects do not affect $\mathbf{v}$ and T in the MHD flow as long as all fluid-wall interfaces are electrically insulating as in the discussed experiment.

The flow under study is characterized by two dimensionless groups, the Hartmann number Ha and the Grashof number Gr:

$$Ha = BL\sqrt{\frac{\sigma}{\rho_0 \nu}},\ Gr = \frac{g\beta\Delta T L^3}{\nu^2}. \tag{5}$$

The former one expresses a dimensionless measure for the strength B of the applied magnetic field and its square gives the ratio of electromagnetic to viscous forces. The Grashof number represents the relative importance of buoyancy and viscous forces. The liquid metal used for experiments has a low Prandtl number, $Pr = \nu\rho_0 c_p/k = 0.029$. In the WCLL blanket the characteristic parameters for ITER TBM and for DEMO reach large values of about $Ha \sim 10^3 - 10^4$ and $Gr \sim 10^8 - 10^{11}$, respectively [2]. In the present study, the selected characteristic numbers are of similar order of magnitude as those in the WCLL TBM.

As kinematic boundary conditions at the fluid-wall interface the no-slip condition, $\mathbf{v} = 0$, applies. The walls of the box and the cylinders are electrically insulating, $\mathbf{j}\cdot\mathbf{n} = 0$. The cavity is assumed ideally adiabatic, $\partial T/\partial n = 0$, while the pipes are kept at differential temperatures $T_{1,2}$.

Since, in the present study, the magnetic Reynolds number is small, $Re_m = \mu\sigma u_0 L \ll 1$, where μ is the magnetic permeability, the problem is solved based on the inductionless approximation according to which the flow-induced magnetic field is negligible compared to the imposed one that remains unaffected by the flow. The quantity u_0 is a characteristic velocity in the problem defined as $u_0 = \rho_0 g\beta\Delta T/\sigma B^2$, which is obtained from a balance of buoyant and electromagnetic forces [18].

Numerical simulations have been performed by using an in-house code based on the finite volume open source code OpenFOAM, in which (1)–(4) have been implemented. A segregated solver has been developed to describe the magneto-convective flow, and the coupling between pressure and velocity is realized by the Pressure-Implicit with Splitting of Operators algorithm. Preconditioned conjugate and bi-conjugate gradient solvers are employed to solve pressure and velocity equations, respectively. The Poisson equation for the electric potential is solved with an algebraic multigrid method. The Lorentz force is treated explicitly and defined at cell-centers. In order to obtain centroid currents to calculate electromagnetic forces, face current fluxes are interpolated in divergence form by using the vector identity $\mathbf{j} = \nabla\cdot(\mathbf{jr})$, where $\mathbf{r}$ is the distance vector [19]. Standard Gaussian finite volume integration is employed for the discretization of convective terms. The code has been validated against a large number of analytical and asymptotic solutions, as well as experimental data [20,21].

Accurate simulations of MHD flows require a proper resolution of the thin boundary layers that form along all walls and of internal layers that develop along magnetic field lines caused for instance by the presence of geometrical discontinuities. In the problem under investigation, internal layers form tangent to the pipes and parallel to the magnetic field. For the present simulations, two topologically different meshes have been used. For small and moderate Hartmann numbers, a structured grid has been employed where points are clustered near the walls and around the planes tangent to the pipes and aligned with $\mathbf{B}$. With the purpose of reducing the total number of computational cells, for simulations of flows under intense magnetic fields, a hybrid grid with local refinement has been generated. It is characterized by boundary-fitted prism layers near the walls of the box and of the cylinders, a regular core mesh and an unstructured region to merge the different grid portions. Three-dimensional simulations with up to $2.5\cdot 10^6$ cells in half of the geometry have been performed on the supercomputers JFRS - 1 at IFERC - CSC and on Marconi - CINECA by using 240 CPUs.

2.3. Recorded electric potential on the walls

The electric potential recorded on the wall of the geometry is given by the difference between the potential $\phi = \phi(\mathbf{x})$ at a point $\mathbf{x}$ on the fluid-wall interface and the one $\phi_r = \phi(\mathbf{x}_r)$ at the reference point $\mathbf{x}_r$ (Fig. 1b). In the following, all quantities taken at the reference point are indicated by the subscript r. When analyzing the wall potential, it is necessary to recall that it is the result of a contribution Φ induced by the liquid metal motion in the magnetic field according to Eq. (4) and an additional thermoelectric part W due to the temperature difference between the measuring points, i.e. $\phi - \phi_r = \Phi - \Phi_r - \left(W(T) - W(T_r)\right)$.

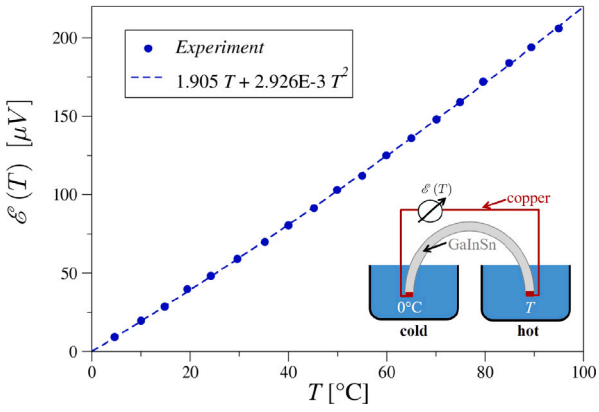

Fig. 2. Experimental data for $\mathscr{E}(T)$ and principle sketch showing the setup.

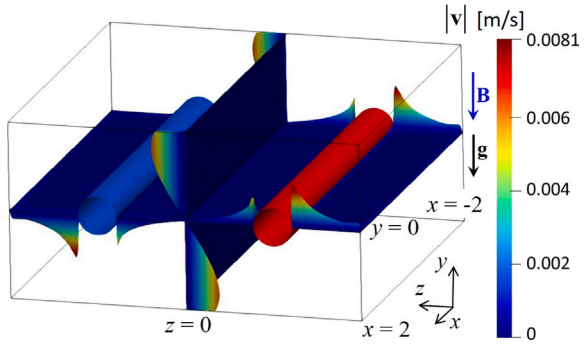

Fig. 3. Velocity distribution on planes $y = 0$ and $z = 0$ colored by the velocity magnitude.

Moreover, in experiments the potential is recorded by a voltmeter that is connected via copper wires to the measuring points on the fluid-wall interface. Therefore, the instrument senses, in addition to the contributions Φ and W, the thermoelectric potential W_w due to the absolute thermoelectric power S_w of the wire material. With abbreviation $\mathscr{E}(T) = W - W_w = \int (S - S_w)\, dT$, the reading of the measuring instrument (subscript m) yields

$$\phi_m - \phi_{m,r} = \Phi - \Phi_r - \left(\mathscr{E}(T) - \mathscr{E}(T_r)\right). \tag{6}$$

As a result, the experimental potential data consists of a flow-induced MHD contribution $\Phi_{MHD} = \Phi - \Phi_r$ and a thermoelectric one $\Phi_{TE} = -\mathscr{E}(T) + \mathscr{E}(T_r)$, both of which are separately accessible by numerical analyses. In the calculations, the potential Φ and the temperature T are calculated and $\mathscr{E}(T)$ is a known almost linear function of T determined experimentally for the liquid metal/wire (GaInSn/Cu) material combination (see Fig. 2). The quantity $\mathscr{E}(T)$ has been determined via a simple experiment where the copper-sealed ends of a thin GaInSn-filled silicon hose were put in two temperature-controlled baths of which the cold one was kept at 0 °C, while the temperature of the hot end was varied in the range $0\ °C < T < 100\ °C$. The voltage has been recorded as in the MHD heat transfer experiment via copper cables. Values obtained from numerical simulations according to Eq. (6) can be then compared with the reading of the instrument.

3. Numerical results

In the following, results for a magneto-convective flow characterized by $Ha = 2000$ ($B = 1.01$ T) and $Gr = 2.5 \cdot 10^7$ ($\Delta T = 17.4$ °C) are discussed. While heat transfer characteristics and temperature distribution have been described already in previous publications [5,11], the present work focuses on a physics-based correct interpretation of electric potential measurements. The main features of the flow are described and the calculated potential distributions along lines on the Hartmann wall and on the end-wall of the box are compared with experimental data.

Fig. 3 shows 3D velocity profiles on a vertical plane at $z = 0$ and on a horizontal one at $y = 0$, colored by the magnitude of velocity. A typical MHD feature is the development of boundary layers with increased velocity at walls parallel to the magnetic field, as visible in the figure close to the end-walls and tangent to the pipes. It can be also seen that the largest convective heat transport occurs in the side layers at the end-walls of the box at $x = \pm 2$, where a jet-like velocity profile is present [5].

In Fig. 4a contours of temperature are displayed on the fluid-wall interface of the cavity. In Fig. 4b the distribution of the normalized temperature is plotted along two vertical lines on the middle plane of the cavity ($z = 0$) near the center of the box at $x = -0.13$ and at the end-walls at $x = \pm 2$. Experimental data recorded at $x = -0.13$ by 11 thermocouples positioned on a central probe (CP) and on the end-wall (EW) are displayed as symbols. A good agreement is found between simulations and experiments. Results reveal a much higher magnitude near the end walls compared to the central position indicating weak thermal convection in the center, and stronger convective motion in the boundary layers close to $x = \pm 2$. In these regions, which serve as closing path for electric currents induced in the core flow [5], the largest potential gradients occur, as shown in Fig. 5a, where contours of electric potential induced by the flow, $\Phi_{MHD} = \Phi - \Phi_r$, are visualized on the liquid metal-wall interface.

As already mentioned in Section 2.3, the measured wall potential is the result of a part induced by the liquid metal motion in the magnetic field, Φ_{MHD}, and a thermoelectric one, Φ_{TE}, due to the temperature difference between measuring points. These two contributions can be evaluated separately in the numerical simulations, while in the experiments thermoelectric effects are intrinsically tied to the non-isothermal operating conditions when recording the electric potential. In Fig. 5b contours of the summation of Φ_{MHD} with the thermoelectric voltage, $\phi = \Phi_{MHD} + \Phi_{TE}$, are displayed on the fluid-wall interface of the cavity. The thermoelectric contribution is about 2.5 times larger than the velocity induced voltage. Contours of Φ_{TE} resemble the temperature field shown in Fig. 4a. It can be clearly seen that in the boundary zones along the end-walls ($x = \pm 2$) ϕ differs more significantly from the temperature distribution due to the stronger convective transport and hence the larger contribution of Φ_{MHD} compared to the core region.

We compare now the experimental data with the potential ϕ obtained by numerical simulations, which contains both flow-induced and thermoelectric voltages. The potential has been normalized by $\phi_0 = u_0 BL$. The position of the lines (E2, H2, H3) along which the results are compared are marked in Fig. 5a. In Fig. 6 data are taken along the line E2 on the end-wall. It can be seen that the thermoelectric voltage gives the largest contribution to the recorded potential data.

In Fig. 7 experimental and numerical results are compared on the Hartmann wall along the lines H2 (a) and H3 (b). The axial profiles (line H2) clearly indicate that there is no flow-induced contribution to the potential in the center of the cavity. Near the end-walls at $x = \pm 2$ the strong convective transport induces a large Φ_{MHD} voltage. It can be also observed that Φ_{MHD} and Φ_{TE} are anti-symmetric and symmetric with respect to $x = 0$, respectively. Therefore the summation ϕ loses its symmetry about $x = 0$. In the transverse z direction (line H3), the measured potential results only from the thermoelectric effects.

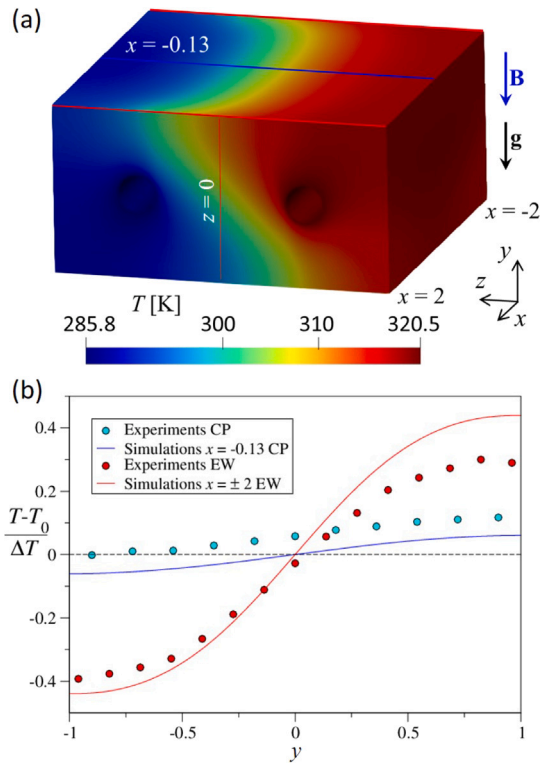

Fig. 4. (a) Temperature contours on the fluid-wall interface. (b) The normalized temperature is plotted along y, in the middle of the cavity ($z = 0$) at $x = -0.13$ and $x = \pm 2$. A comparison with experimental data (symbols) is shown.

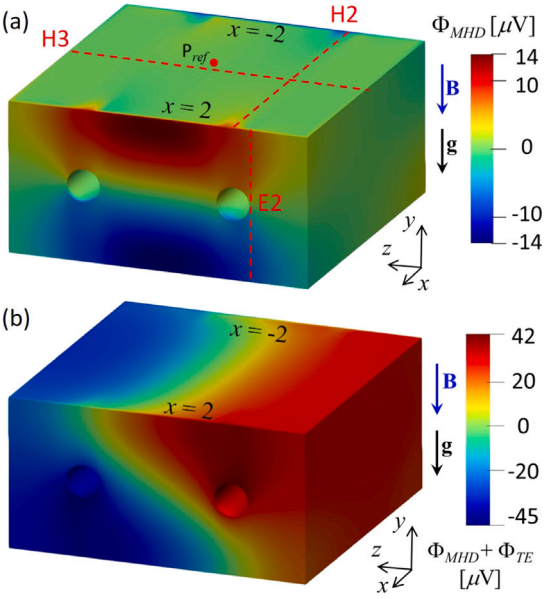

Fig. 5. Contours of calculated flow-induced electric potential Φ_{MHD} (a) and summation $\Phi_{MHD}+\Phi_{TE}$ with the thermoelectric contribution. The position P_{ref} marks the reference point $\mathbf{x}_r$ used to measure the electric potential.

In the experiments, the recorded potential values are often smaller than the calculated ones. This could be related to parasitic heat losses across the walls of the test-section, which may result in somewhat smaller temperature gradients, as shown in Fig. 4b, thereby leading to a slightly reduced thermoelectric contribution.

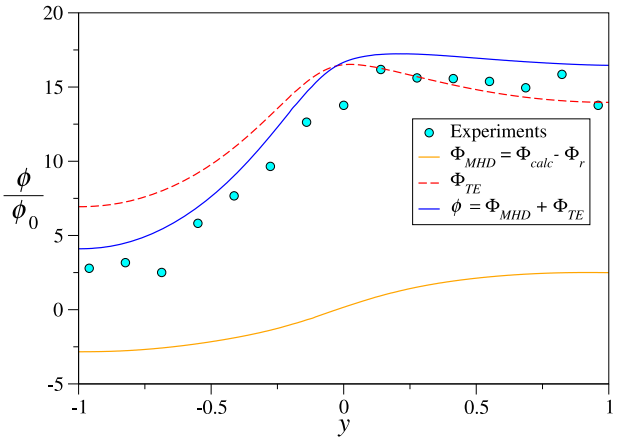

Fig. 6. Experimental data (symbols) are compared with the numerical results along the vertical line E2 (see Fig. 5a). Φ_{MHD} is the velocity-induced potential, Φ_{TE} the thermoelectric voltage.

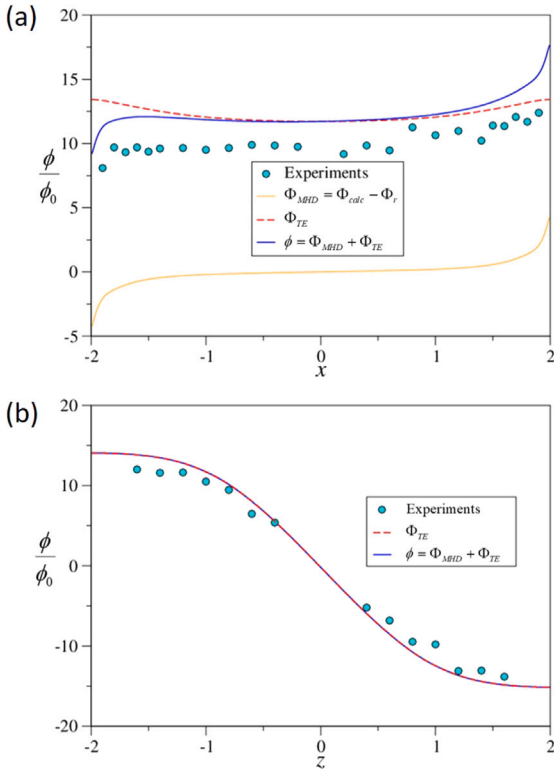

Fig. 7. Experimental data (symbols) are compared with numerical results along lines H2 (a) and H3 (b) on the Hartmann wall (see Fig. 5a). Φ_{MHD} is the flow-induced potential, Φ_{TE} the thermoelectric voltage.

4. Concluding remarks

Magneto-convection in a liquid metal has been investigated numerically and experimentally in a model geometry consisting of a rectangular cavity in which two parallel pipes are inserted and kept at constant differential temperatures. A magnetic field is applied perpendicular to the axis of the cylinders and to two walls of the box. A balance between electromagnetic and buoyant forces determines flow and temperature distributions in the cavity [5,11]. The major result of the present work is that measurements of electric potential in MHD convective flows is always significantly affected by thermoelectric effects, since measured data is given by the voltage between two electrodes that are at different temperatures. The thermoelectric potential depends on the temperature and on the material of the conductors and it is superimposed on the potential induced by the motion of the liquid metal through the magnetic field. In order to use the recorded potential on the walls to reconstruct velocity features of the convective flow, as done in isothermal MHD flows, flow-induced electric potential and thermoelectric contribution have to be separated. Since the latter is intrinsically related to the measuring method and to the non-isothermal conditions in the convective flow, the proper interpretation of recorded data would require simultaneous measurements of temperature and potential at each electrode. However, having copper electrodes and thermocouples exactly at the same position is not possible. For these reasons only numerical simulations, in which flow-induced electric potential and thermoelectric voltage can be estimated separately, may shed light into the problem. By taking into account the thermoelectric potential in the numerical results in addition to the velocity-induced part, a good agreement between experiments and simulations is found.

CRediT authorship contribution statement

C. Mistrangelo: Conceptualization, Data curation, Formal analysis, Investigation, Methodology, Software, Validation, Visualization, Writing – original draft, Writing – review & editing. **L. Bühler:** Conceptualization, Methodology, Writing – review & editing. **C. Courtessole:** Data curation, Investigation, Writing – review & editing. **C. Koehly:** Writing – review & editing.

Declaration of competing interest

The authors declare that they have no known competing financial interests or personal relationships that could have appeared to influence the work reported in this paper.

Data availability

The authors do not have permission to share data.

Acknowledgments

This work has been carried out within the framework of the EUROfusion Consortium, funded by the European Union via the Euratom Research and Training Programme (Grant Agreement No 101052200 — EUROfusion). Views and opinions expressed are however those of the author(s) only and do not necessarily reflect those of the European Union or the European Commission. Neither the European Union nor the European Commission can be held responsible for them.

References

[1] S. Smolentsev, R. Moreau, L. Bühler, C. Mistrangelo, MHD thermofluid issues of liquid-metal blankets: Phenomena and advances, Fusion Eng. Des. 85 (2010) 1196–1205.

[2] C. Mistrangelo, L. Bühler, S. Smolentsev, V. Klüber, I. Maione, J. Aubert, MHD flow in liquid metal blankets: major design issues, MHD guidelines and numerical analysis, Fusion Eng. Des. 173 (2021) 112795, http://dx.doi.org/10.1016/j.fusengdes.2021.112795.

[3] G. Federici, L. Boccaccini, F. Cismondi, M. Gasparotto, Y. Poitevin, I. Ricapito, An overview of the EU breeding blanket design strategy as an integral part of the DEMO design effort, Fusion Eng. Des. 141 (2019) 30–42, http://dx.doi.org/10.1016/j.fusengdes.2019.01.141.

[4] A. Del Nevo, P. Arena, G. Caruso, P. Chiovaro, P.D. Maio, M. Eboli, F. Edemetti, N. Forgione, R. Forte, A. Froio, F. Giannetti, G.D. Gironimo, K. Jiang, S. Liu, F. Moro, R. Mozzillo, L. Savoldi, A. Tarallo, M. Tarantino, A. Tassone, M. Utili, R. Villari, R. Zanino, E. Martelli, Recent progress in developing a feasible and integrated conceptual design of the WCLL BB in EUROfusion project, Fusion Eng. Des. 146 (2019) 1805–1809, http://dx.doi.org/10.1016/j.fusengdes.2019.03.040.

[5] C. Mistrangelo, L. Bühler, H.-J. Brinkmann, C. Courtessole, V. Klüber, C. Koehly, Magneto-convective flows around two differentially heated cylinders, Heat Mass Transf. 59 (2023) 2005–2021, http://dx.doi.org/10.1007/s00231-023-03350-2.

[6] U. Burr, U. Müller, Rayleigh-Bénard convection in liquid metal layers under the influence of a vertical magnetic field, Phys. Fluids 13 (11) (2001) 3247–3257.
[7] K. Okada, H. Ozoe, Experimental heat transfer rates of natural convection of molten gallium suppressed under an external magnetic field in either the x, y, or z direction, J. Heat Transfer 114 (1992) 107–114, http://dx.doi.org/10.1115/1.2911234.
[8] O. Zikanov, I. Belyaev, Y. Listratov, P. Frick, N. Razuvanov, V. Sviridov, Mixed convection in pipe and duct flows with strong magnetic fields, Appl. Mech. Rev. 73 (2021) http://dx.doi.org/10.1115/1.4049833, 010801–1–35.
[9] L. Bühler, C. Mistrangelo, MHD flow and heat transfer in model geometries for WCLL blankets, Fusion Eng. Des. 122 (2017) 919–923, http://dx.doi.org/10.1016/j.fusengdes.2017.01.014.
[10] C. Koehly, L. Bühler, C. Mistrangelo, Design of a test section to analyze magneto-convection effects in WCLL blankets, Fusion Sci. Technol. 75 (2019) 1010–1015, http://dx.doi.org/10.1080/15361055.2019.1607705.
[11] C. Courtessole, H.-J. Brinkmann, L. Bühler, Experimental investigation of magneto-convective flows around two differentially heated cylinders, J. Fluid Mech. (2023) submitted for publication.
[12] C.B. Reed, B.F. Picologlou, P.V. Dauzvardis, J.L. Bailey, Techniques for measurement of velocity in liquid-metal MHD flows, Fusion Technol. 10 (1986) 813–821.
[13] L. Bühler, B. Lyu, H.-J. Brinkmann, C. Mistrangelo, Reconstruction of 3D MHD liquid metal velocity from measurements of electric potential on the external surface of a thick-walled pipe, Fusion Eng. Des. 168 (2021) 112590, http://dx.doi.org/10.1016/j.fusengdes.2021.112590.
[14] J.A. Shercliff, Thermoelectric magnetohydrodynamics, J. Fluid Mech. 91 (1979) 231–251.
[15] T. Weissenfluh, Probes for local velocity and temperature measurements in liquid metal flow, Int. J. Heat Mass Transfer 28 (8) (1985) 1563–1574.
[16] Y. Plevachuk, V. Sklyarchuk, S. Eckert, G. Gerbeth, R. Novakovic, Thermophysical properties of the liquid ga-in-sn eutectic alloy, J. Chem. Eng. Data 59 (3) (2014) 757–763, http://dx.doi.org/10.1021/je400882q, arXiv:10.1021/je400882q.
[17] J.A. Shercliff, Thermoelectric magnetohydrodynamics in closed containers, Phys. Fluids 22 (4) (1979) 635–640.
[18] L.N. Hjellming, J.S. Walker, Melt motion in a czochralski crystal puller with an axial magnetic field: motion due to buoyancy and thermocapillarity, J. Fluid Mech. 182 (1987) 335–368.
[19] M.-J. Ni, R. Munipalli, P. Huang, N.B. Morley, M.A. Abdou, A current density conservative scheme for incompressible MHD flows at a low magnetic Reynolds number. Part II: On an arbitrary collocated mesh, J. Comput. Phys. 227 (1) (2007) 205–228.
[20] S. Smolentsev, S. Badia, R. Bhattacharyay, L. Bühler, L. Chen, Q. Huang, H.-G. Jin, D. Krasnov, D.-W. Lee, E. Mas de les Valls, C. Mistrangelo, R. Munipalli, M.-J. Ni, D. Pashkevich, A. Patel, G. Pulugundla, P. Satyamurthy, A. Snegirev, V. Sviridov, P. Swain, T. Zhou, O. Zikanov, An approach to verification and validation of MHD codes for fusion applications, Fusion Eng. Des. 100 (2015) 65–72, http://dx.doi.org/10.1016/j.fusengdes.2014.04.049.
[21] V. Klüber, L. Bühler, C. Mistrangelo, Numerical investigation of liquid metal flow in square channels under inclined magnetic fields for fusion relevant parameters, Magnetohydrodynamics 56 (2020) 149–156, http://dx.doi.org/10.22364/mhd.56.2-3.6.